# Design, Fabrication, Measurement, and Analysis of Mach-Zhender Interferometers on a Silicon Photonic Chip

Sam Hardy (EdEx UN: Sam_H_251)

## Abstract

We summarize the theory, design, fabrication, measurement, and analysis of five Mach-Zehnder Interferometers (MZI's) from a silicon-photonic integrated circuit built on a chip. Each MZI is unbalanced, with a range of path length differences ($\Delta L$). The waveguide group index ($n_g$) is extracted from experimental data, and compared with simulated values. Agreement of <1% is observed, and is within the error margins of manufacturing variability.

## 1. Introduction

The Mach-Zehnder Interferometer (MZI) is a basic photonic component that modulates an input electric field amplitude (such as laser light intensity) via a relative phase difference. The field is split into two paths of different lengths, such that a percentage of constructive interference occurs upon recombination at the output. The MZI has practical applications in optical switches, electro-optical and thermal modulators, and filters, to name a few.

In this study, we create five MZI's, each with a unique path length imbalance ($\Delta L$). We choose imbalances of 50um, 75um, 100um, 125um, and 150um. These MZI's are designed in KLayout, simulated with LUMERICAL software, fabricated at Applied Nanotools, measured at the University of British Columbia, and the experimental data analyzed with MATLAB to determine group index ($n_g$). The simulated and experimental data is compared.

## 2. Theory

A simple schematic for an imbalanced MZI is shown in Figure 1. Light is split into two separate paths of unequal length ($L_1 \neq L_2$), then recombined. This path length imbalance can be realized by either inherent physical length differences (passive), or by introducing optical path length differences by varying the refractive index of one or both of the paths, via temperature changes (local thermal application) or applying external electric fields (active).

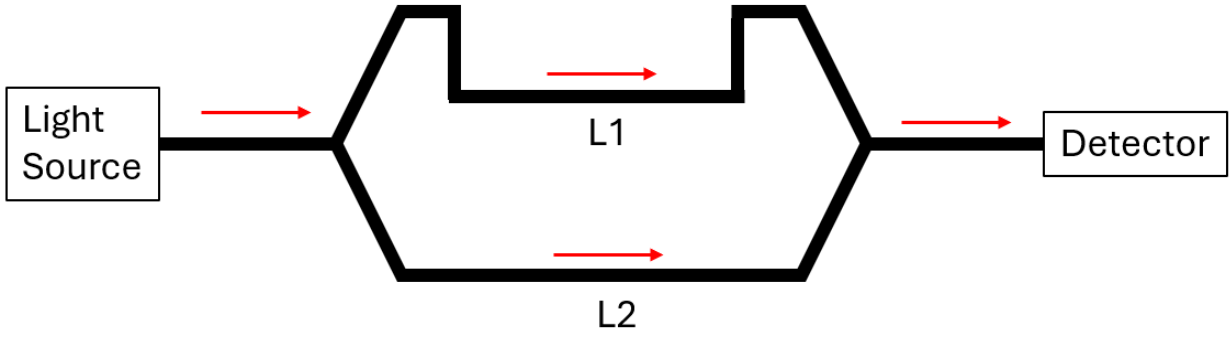


*Figure 1: Imbalanced MZI, with $L_1 \neq L_2$*

When recombined, the output intensity is given by the equation [1]:

$$I_o = \frac{I_i}{2}[1 + \cos(\beta \Delta L)] \quad \text{where } \beta = \frac{2\pi n}{\lambda} \quad [1]$$

Note that the propagation constant ($\beta$) is the same for both waveguides.

## 3. Modeling and Simulation

For our MZI's, we chose silicon ($Si$) slab waveguides embedded in a silicon dioxide ($SiO_2$) substrate. Light is guided along the higher-index $Si$ material. We chose slab waveguides that are 500nm wide and 220nm thick. Figure 2 shows a cross-section of this waveguide, along with the mode profiles for the first TE ($TE_0$) and TM ($TM_0$) modes at 1550nm wavelength light. We can see that the mode is well-confined for $TE_0$, and we will only be focusing on this polarization orientation for this report.

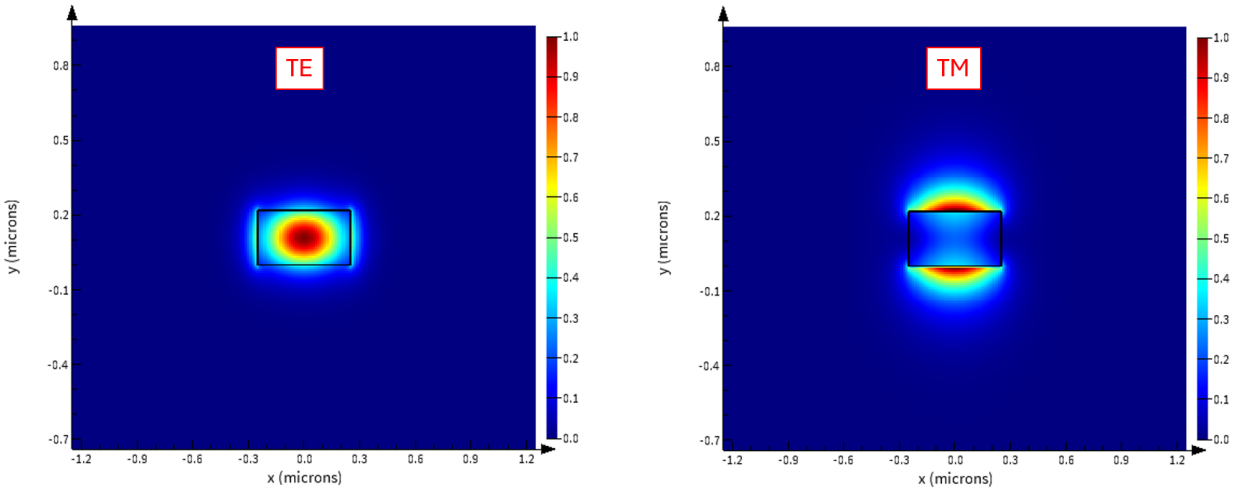


*Figure 2: Profile of the $TE_0$ and $TM_0$ modes, with respect to the waveguide (rectangle)*

The effective and group indices ($n_{eff}, n_g$) are also extracted, which describe how light propagates down the waveguide. These are plotted in Figure 3.

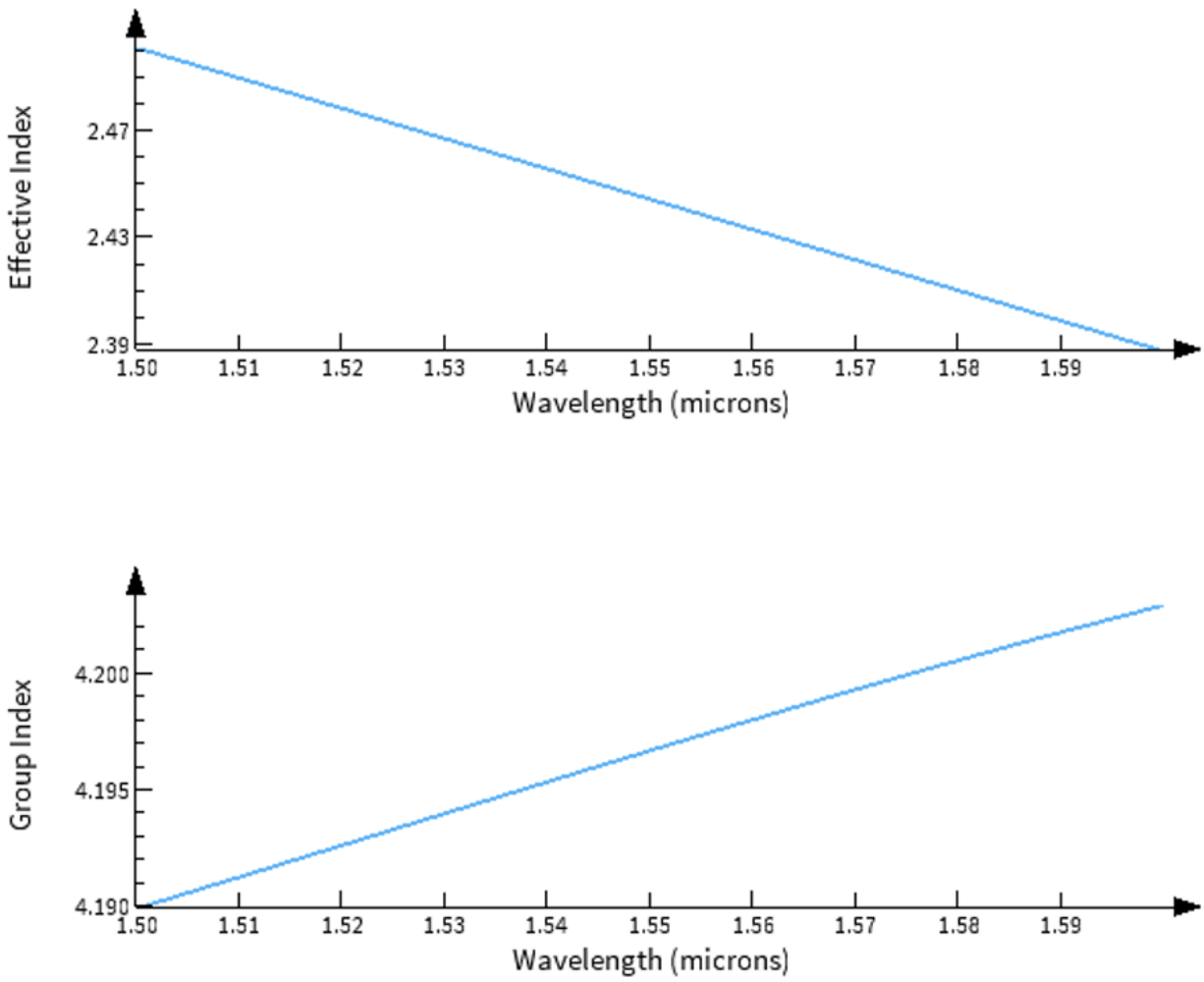


*Figure 3: $n_{eff}, n_g$ as a function of wavelength*

At the 1550nm wavelength of interest, $n_{eff} \approx 2.44$ and $n_g \approx 4.2$.

Another way to model optical structures is by using a compact model. A compact model is a polynomial equation that describes $n_{eff}$ as a function of wavelength. See equation [2]:

$$n_{eff} = n_1 + n_2(\lambda - \lambda_0) + n_3(\lambda - \lambda_0)^2 \quad [2]$$

For our chosen slab waveguide (500nm by 220nm), $\lambda_0 = 1550nm, n_1 = 2.44,\ n_2 = -1.13,\ n_3 = -0.042$. These coefficients were obtained by curve fitting the effective index in LUMERICAL MODE.

Returning to equation [1], we see that the MZI transfer function depends on wavelength $\lambda$. Its response varies in a sinusoidal fashion as a function of wavelength. See Figure 4.

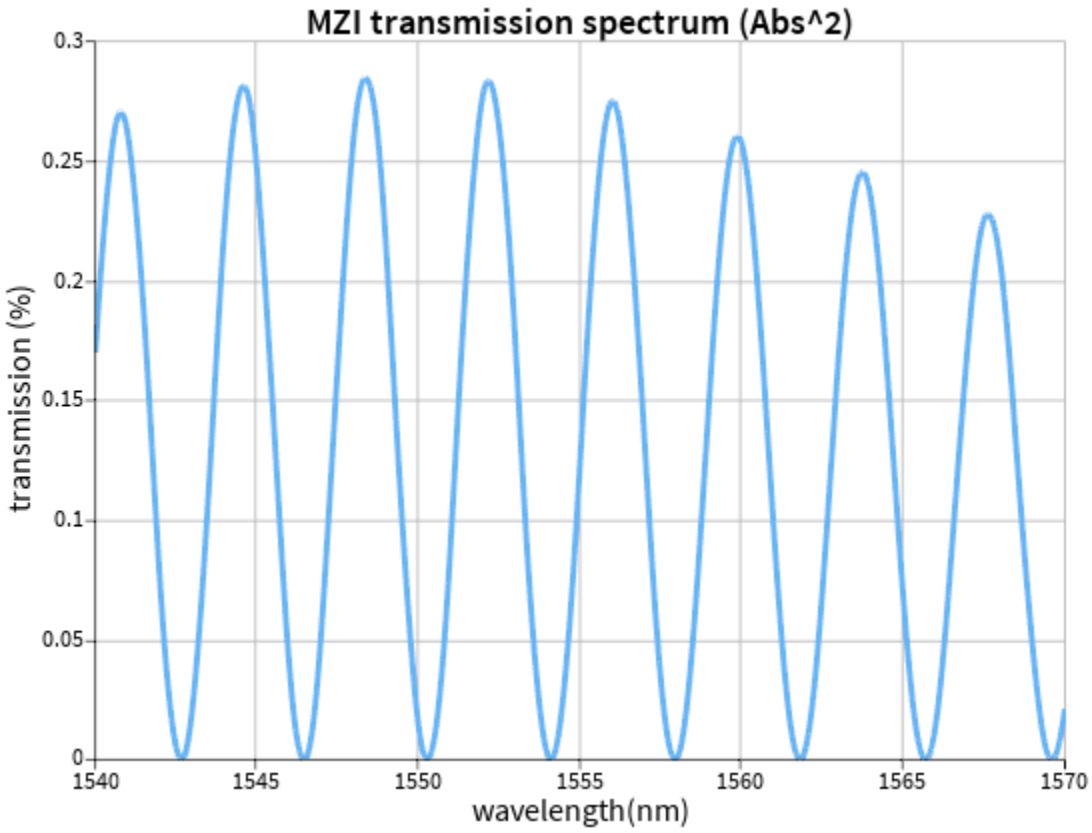

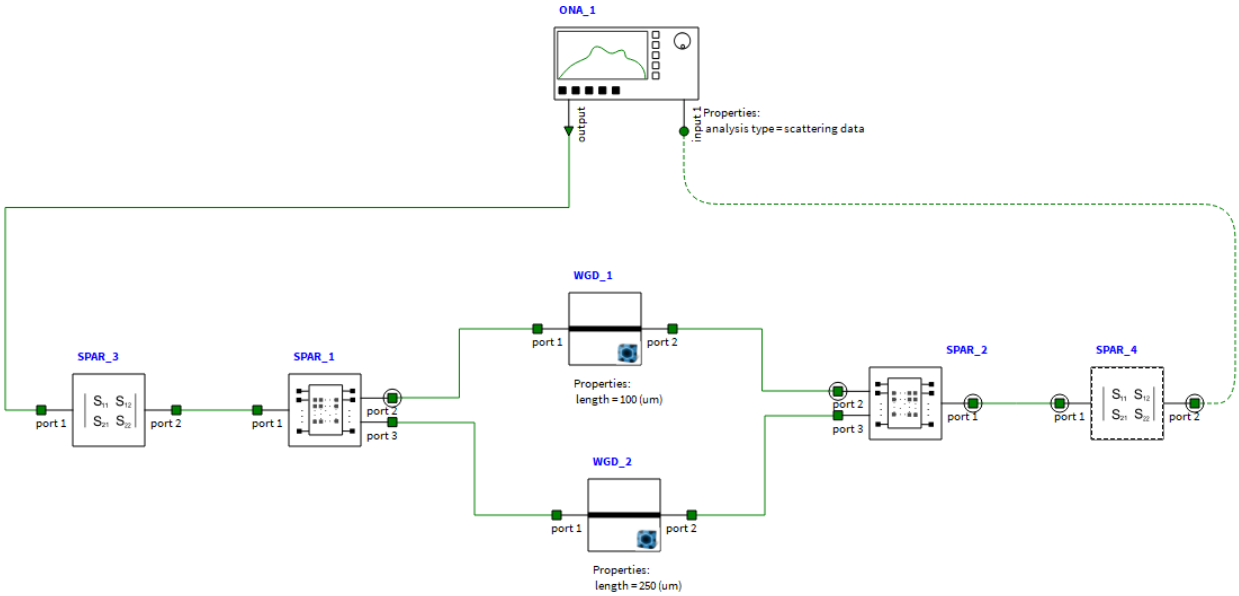


*Figure 4: Transmission spectrum, for $\Delta L = 150um$, and corresponding LUMERICAL INTERCONNECT circuit*

The distance between peaks is an important parameter, called the free spectral range (FSR). FSR is inversely proportional to the path length difference ($\Delta L$) in the interferometer, as we can see in equation [3]. A short distance between peaks means a small FSR, and a larger $\Delta L$.

$$FSR = \frac{\lambda^2}{n_g \Delta L} \quad [3]$$

In this study, we will use 5 different values for $\Delta L$. These are summarized in Table 1, along with expected FSR values from equation [3].

| ΔL (um) | FSR (nm) |
|---|---|
| 50 | 11.44 |
| 75 | 7.63 |
| 100 | 5.72 |
| 125 | 4.58 |
| 150 | 3.81 |

*Table 1: FSR and $\Delta L$ at 1550nm*

Finally, we will use the values of FSR obtained from experimentation, along with the corresponding $\Delta L$, to determine $n_g$, again from equation [3].

As an example, we see that the FSR in Figure [4] is 3.84nm (distance between adjacent peaks, 1556.01nm - 1552.17nm), for $\Delta L$ = 150um, at $\lambda$ = 1550nm. We plug these into equation [3] to get $n_g$ = 4.17, which is in good agreement with the value of 4.2 from Figure 3.

The above simulations were developed into a design using KLayout software. The layout mask is shown in Figure 5. It contains five MZI devices for TE polarization, each with a different path length difference, plus three loopback structures of different length for de-embedding purposes and modeling propagation loss. All grating couplers have a 127um pitch spacing, and all waveguides have a 5um bend radius in order to minimize loss for TE polarized light. A list of the devices (ie device manifest) is included in Table 2, along with simulated values for FSR from Lumerical Interconnect. These simulated values are updated from Table 1, to account for the presence of real grating couplers, and waveguide bend radii. The values are in good agreement with the waveguide values from Table 1.

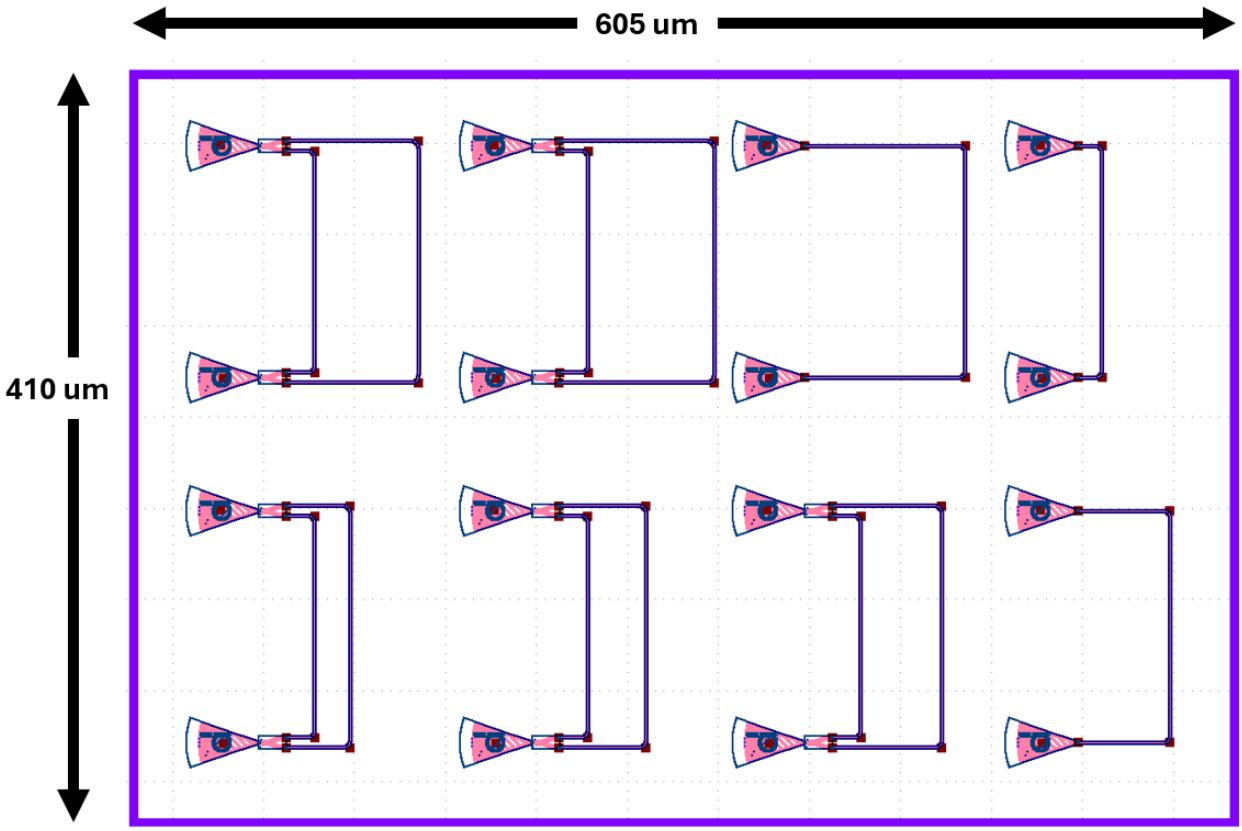


*Figure 5: Layout mask for fabrication*

| Device Label | Device Type | ΔL (um) | Simulated FSR (nm) |
|---|---|---|---|
| MZI1 | MZI | 50 | 11.44 |
| MZI2 | MZI | 75 | 7.68 |
| MZI3 | MZI | 100 | 5.73 |
| MZI4 | MZI | 125 | 4.6 |
| MZI5 | MZI | 150 | 3.83 |
| MZI_deembed_woy_150 | de-embed | N/A | N/A |
| MZI_deembed_woy_225 | de-embed | N/A | N/A |
| MZI_deembed_woy_300 | de-embed | N/A | N/A |

*Table 2: Device manifest*

## 4. Fabrication

The design in Figure 5 was fabricated onto a chip at Applied Nanotools Inc in Edmonton, Canada. The process steps are summarized in Figure 6, along with a scanning electron microscope (SEM) image of a grating coupler and waveguide, and are as follows:

1. A negative photo-resist layer is spun and baked onto a silicon-on-insulator (SOI) wafer substrate.
2. The resist is exposed to an electron beam, which draws the device patterns (Electron Beam Lithography (EBL) [1]).
3. The patterns are developed via immersion in hydroxide.
4. The wafer is rinsed, dried, and then the unexposed areas are removed via plasma etching.
5. Oxide is deposited to act as a cladding.
6. The wafer is diced into chips.

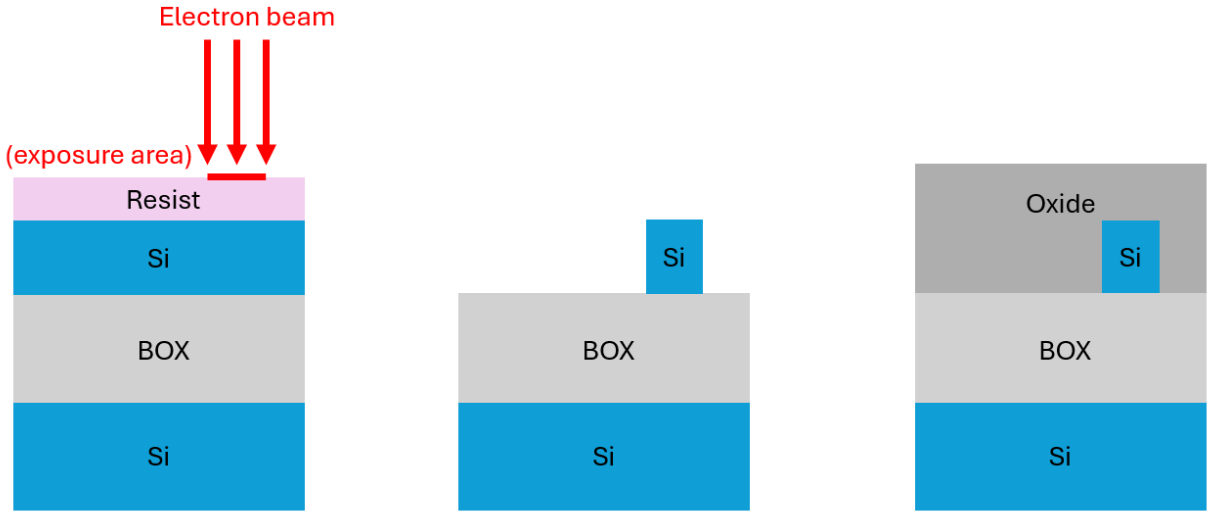

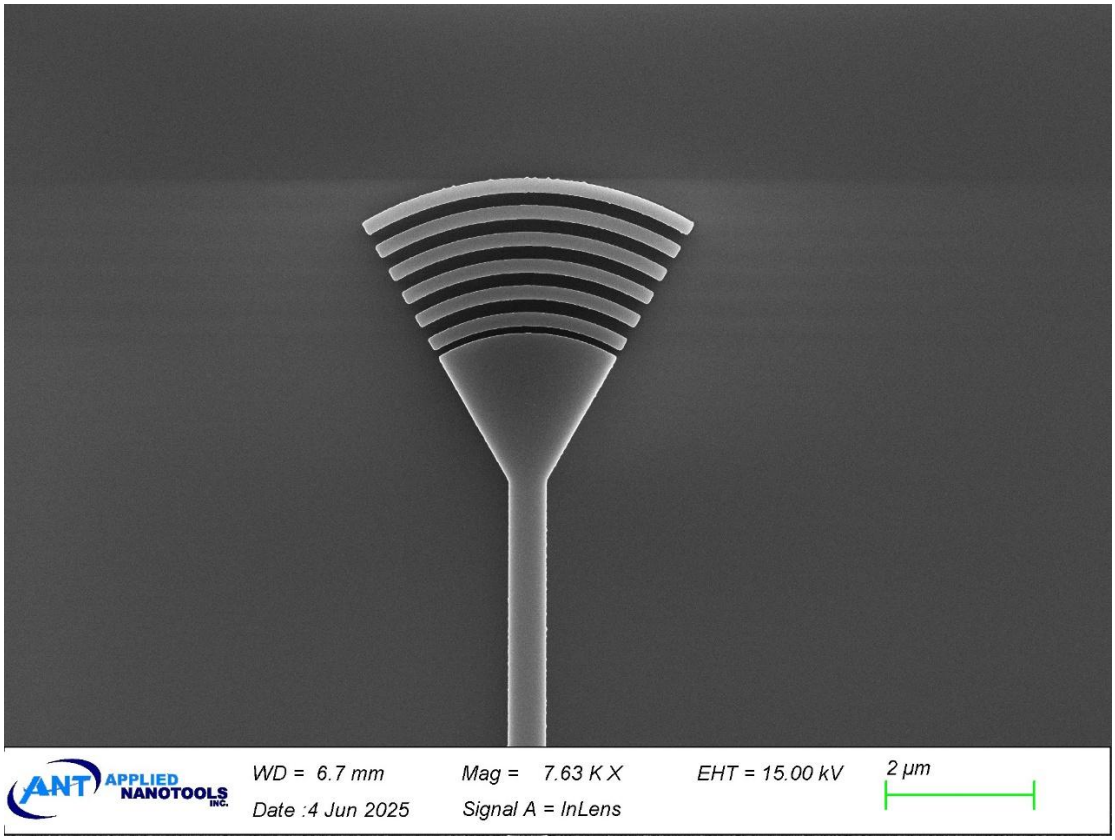


*Figure 6: EBL fabrication process and SEM photograph*

The full fabrication description is provided for reference:

> The photonic devices were fabricated using the NanoSOI MPW fabrication process by Applied Nanotools Inc. [7] which is based on direct-write 100 keV electron beam lithography technology. Silicon-on-insulator wafers of 200 mm diameter, 220 nm device thickness and 2 µm buffer oxide thickness are used as the base material for the fabrication. The wafer was pre-diced into square substrates with dimensions of 25x25 mm, and lines were scribed into the substrate backsides to facilitate easy separation into smaller chips once fabrication was complete. After an initial wafer clean using piranha solution (3:1 H2SO4:H2O2) for 15 minutes and water/IPA rinse, hydrogen silsesquioxane (HSQ) resist was spin-coated onto the substrate and heated to evaporate the solvent. The

photonic devices were patterned using a JEOL JBX-8100FS electron beam instrument at The University of British Columbia. The exposure dosage of the design was corrected for proximity effects that result from the backscatter of electrons from exposure of nearby features. Shape writing order was optimized for efficient patterning and minimal beam drift. After the e-beam exposure and subsequent development with a tetramethylammonium sulfate (TMAH) solution, the devices were inspected optically for residues and/or defects. The chips were then mounted on a 4" handle wafer and underwent an anisotropic ICP-RIE etch process using chlorine after qualification of the etch rate. The resist was removed from the surface of the devices using a 10:1 buffer oxide wet etch, and the devices were inspected using a scanning electron microscope (SEM) to verify patterning and etch quality. A 2.2 μm oxide cladding was deposited using a plasma-enhanced chemical vapour deposition (PECVD) process based on tetraethyl orthosilicate (TEOS) at 300°C. Reflectrometry measurements were performed throughout the process to verify the device layer, buffer oxide and cladding thicknesses before delivery.

As with all fabrication processes, there are manufacturing variabilities with EBL. There will be deviations from dimensions defined in a design, versus what is physically built. This is due to several factors, such as resist imperfections (thickness non-uniformity, age), e-beam exposure and plasma etching errors, to name a few. Information about these variations is typically provided by the supplier/manufacturer, such that a distribution of waveguide widths and thicknesses can be predicted. For our nominal waveguide dimensions of 500nm width and 220 nm thick, we can expect a range of widths from 470nm to 510nm, and a range of thicknesses from 215.3nm to 223.1nm. A simple way to account for manufacturing variations is to perform a corner analysis, which means repeating simulations beyond the nominal values. Namely, we calculate the effective and group refractive indices versus wavelength for TE polarization across the range of waveguide widths and thicknesses. We adopt the "fast (F)-slow (S)-typical (T)" nomenclature from semiconductor process control to denote the corners. For example, typical-typical (TT) denotes 500nm x 220nm, and fast-slow (FS) denotes 510nm x 215.3nm. This schematic, along with the results, is shown in Figure 7.

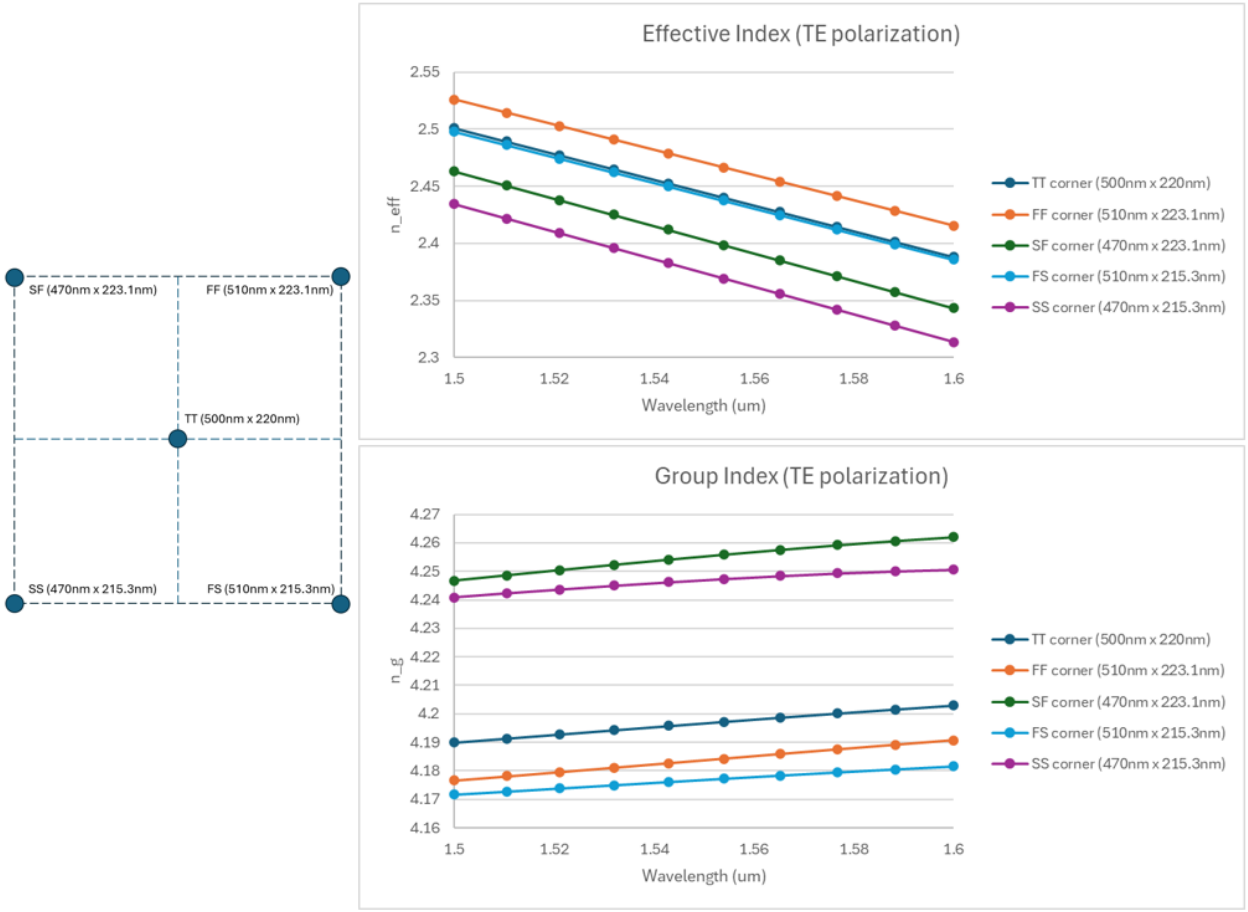


*Figure 7: Corner analysis for effective and group index vs wavelength*

We also summarize the results for the corner analysis in Table 3, for the case of 1550 nm wavelength, and expand to include effective index compact model coefficients from equation [2].

| Corner | ng at 1550 for TE | neff at 1550 for TE | neff compact model coeffs (n1, n2, n3, λ0) |
|---|---|---|---|
| TT | 4.1967 | 2.44457 | 2.44457, -1.13036, -0.0423127, 1.55 |
| FF | 4.1837 | 2.4709 | 2.47088, -1.10503, -0.04564, 1.55 |
| SF | 4.2553 | 2.4034 | 2.4034, -1.1946, -0.0503126, -1.55 |
| FS | 4.1768 | 2.4419 | 2.44191, -1.11924, -0.0325157, 1.55 |
| SS | 4.24696 | 2.3741 | 2.37409, -1.20811, -0.0322388, 1.55 |

*Table 3: Corner analysis for effective and group index at 1550 nm wavelength, TE polarization, along with compact model coefficients*

Finally, we input the results from this waveguide corner analysis into the analytical expression for FSR (equation [3]), and compare with MZI circuit simulations (using the circuit schematic from Figure 4, with swapping in/out the corner TT, SF, etc component waveguides). See Table 4. We can see that there is generally better agreement of the methods as $\Delta L$ increases.

| Corner | ΔL (um) | FSR from eqn (nm) | FSR from model (nm) | eqn - model diff (nm) |
|---|---|---|---|---|
| TT | 50 | 11.45 | 11.37 | 0.079 |
| FF | 50 | 11.49 | 11.41 | 0.075 |
| SF | 50 | 11.29 | 11.22 | 0.072 |
| FS | 50 | 11.50 | 11.43 | 0.074 |
| SS | 50 | 11.31 | 11.24 | 0.074 |
| TT | 75 | 7.63 | 7.6 | 0.033 |
| FF | 75 | 7.66 | 7.62 | 0.037 |
| SF | 75 | 7.53 | 7.48 | 0.048 |
| FS | 75 | 7.67 | 7.65 | 0.019 |
| SS | 75 | 7.54 | 7.53 | 0.013 |
| TT | 100 | 5.72 | 5.71 | 0.015 |
| FF | 100 | 5.74 | 5.72 | 0.023 |
| SF | 100 | 5.65 | 5.62 | 0.026 |
| FS | 100 | 5.75 | 5.73 | 0.022 |
| SS | 100 | 5.66 | 5.63 | 0.027 |
| TT | 125 | 4.58 | 4.57 | 0.010 |
| FF | 125 | 4.59 | 4.58 | 0.014 |
| SF | 125 | 4.52 | 4.51 | 0.007 |
| FS | 125 | 4.60 | 4.59 | 0.012 |
| SS | 125 | 4.53 | 4.51 | 0.016 |
| TT | 150 | 3.82 | 3.81 | 0.006 |
| FF | 150 | 3.83 | 3.82 | 0.008 |
| SF | 150 | 3.76 | 3.75 | 0.014 |
| FS | 150 | 3.83 | 3.83 | 0.005 |
| SS | 150 | 3.77 | 3.77 | 0.001 |

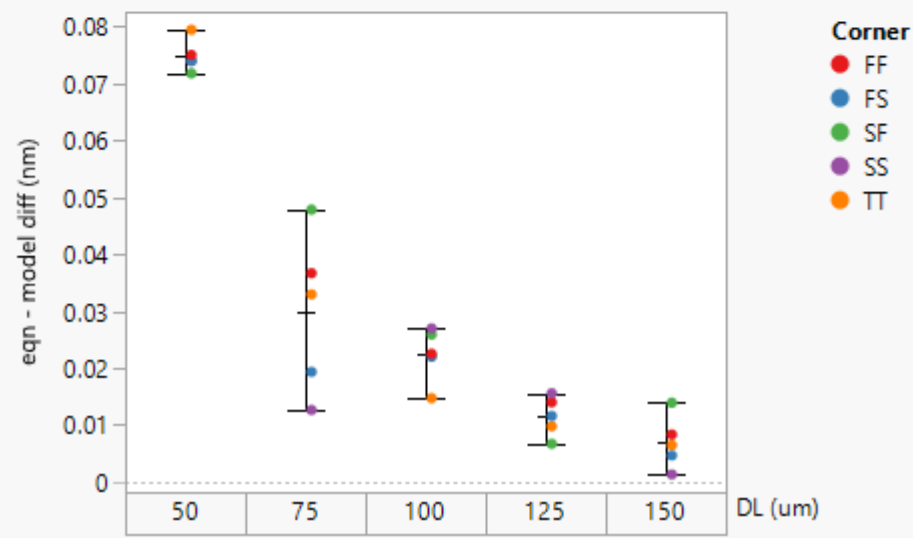


*Table 4: Waveguide corner analysis effect on circuit FSR.*

## 5. Experimental Data

The measurement of the devices designed and modeled above was performed on an automated test setup at the University of British Columbia [2, 6], which consists of an Agilent 81600B tunable laser (10 pm step size, swept from 1500 nm to 1600 nm), an Agilent 81635A optical power meter, and control software written in Python [3]. Polarization-maintaining (PM) fibers were used to couple TE light into and out of the grating couplers and waveguides [4, 5]. A summary of the raw transmission data is plotted in Figure 8.

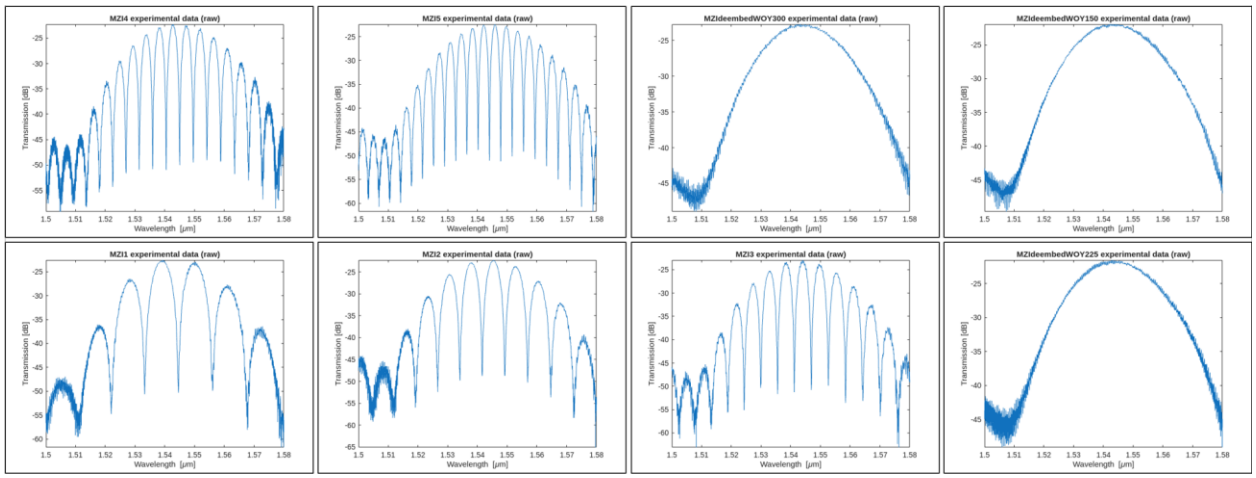


*Figure 8: plots of raw data, organized same as layout mask in Figure 5*

## 6. Analysis

In order to characterize the fabricated MZIs from their experimental data, we first perform some post-processing steps on the raw data. First, we de-embed the effect of the grating couplers, in order to isolate the performance of the MZI itself. This is done by background subtracting the spectrum from one of the loopback structures from each MZI. An example for MZI1 is shown in Figure 9. We chose to use the same loopback for de-embedding for each MZI, namely the one that is 150 microns in length (MZIdeembedWOY150). The reason is that for all 5 MZI's, one arm is held at a fixed length of 150 microns, so this length is consistent across all MZI devices. To reduce noise effects on the edges of the spectrum, only loopback data that is within 10 dB of the peak power was considered.

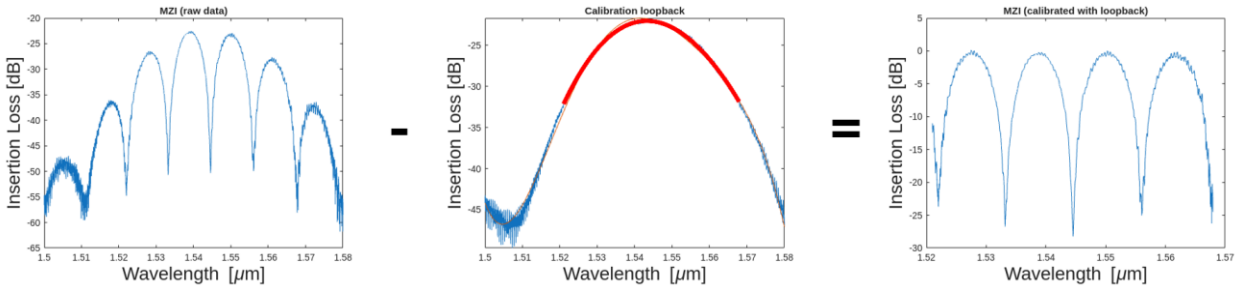


*Figure 9: MZI1 spectrum before and after de-embedding. ie MZI1 minus MZIdeembedWOY150 equals flattened specrta*

Next, we curve fit the flattened spectrum, using autocorrelation in MATLAB to sweep the spectrum with itself (ie apply a range of shift offsets, or "lags"). In this way, we obtain clean values for the peak-to-peak distance, or FSR. An example of this for MZI2 is shown in Figure 10.

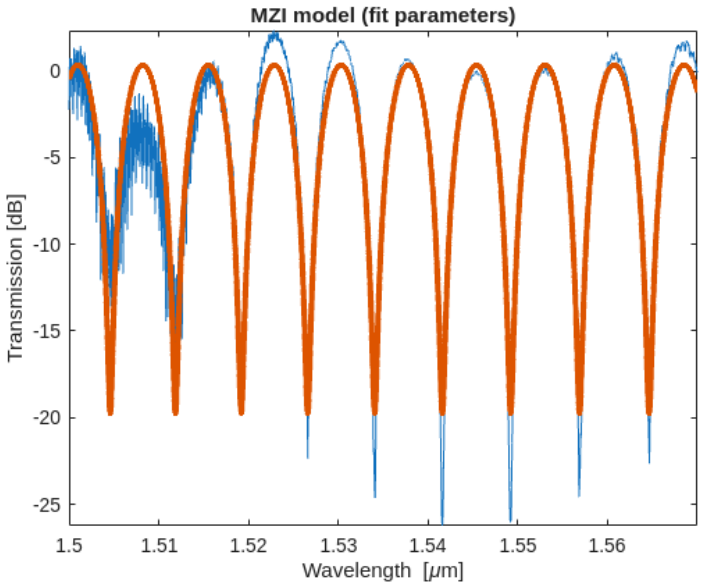


*Figure 10: MZI2 curve fitting from autocorrelation*

Since we know the path length difference of each device, we know the group index as well. The full list of experimental results, along with comparison with simulations, is summarized in Table 5.

| DEVICE | ΔL (um) | FSR (simulated, nm) | FSR (experiment, nm) | FSR % diff | $n_g$ (simulated, nm) | $n_g$ (experiment, nm) | $n_g$ % diff |
|---|---|---|---|---|---|---|---|
| MZI1 | 50 | 11.44 | 11.37 | 0.614 | 4.2002 | 4.175 | 0.602 |
| MZI2 | 75 | 7.68 | 7.55 | 1.707 | 4.171 | 4.191 | 0.478 |
| MZI3 | 100 | 5.73 | 5.66 | 1.23 | 4.193 | 4.174 | 0.454 |
| MZI4 | 125 | 4.6 | 4.53 | 1.53 | 4.178 | 4.192 | 0.335 |
| MZI5 | 150 | 3.83 | 3.8 | 0.786 | 4.182 | 4.1915 | 0.227 |

*Table 5: Summary of simulation and experimental results.*
*500nm x 220nm waveguides, TE mode, wavelength = 1550 nm*

We observe good agreement for simulated and experimental values, within 1 percent for the group index of refraction. And the agreement gets better for larger ΔL. Finally, we see that our experimental values lie within the error margins of manufacturing variability established from our corner analysis (for both analytic and modeled values, Table 4).

In addition, we used the three de-embed loopbacks to get an estimate of the propagation loss for TE light at 1550nm. See Figure 11 for the overlayed spectra (excluding noisy/low power tails), and fitted curves. We see that by increasing the loopback length from 150 um to 300 um, we pick up 0.8 dB of loss (since units of dBm minus dBm results in dB). So the propagation loss is 0.8dB per 150um, or 53 dB/cm. This quick back-of-the-envelope calculation is in close agreement with results obtained from a more thorough cutback analysis in Matlab (49 dB/cm), also in Figure 11. This is much higher than the expected value for TE waveguides of ~10 dB/cm, so further study is needed.

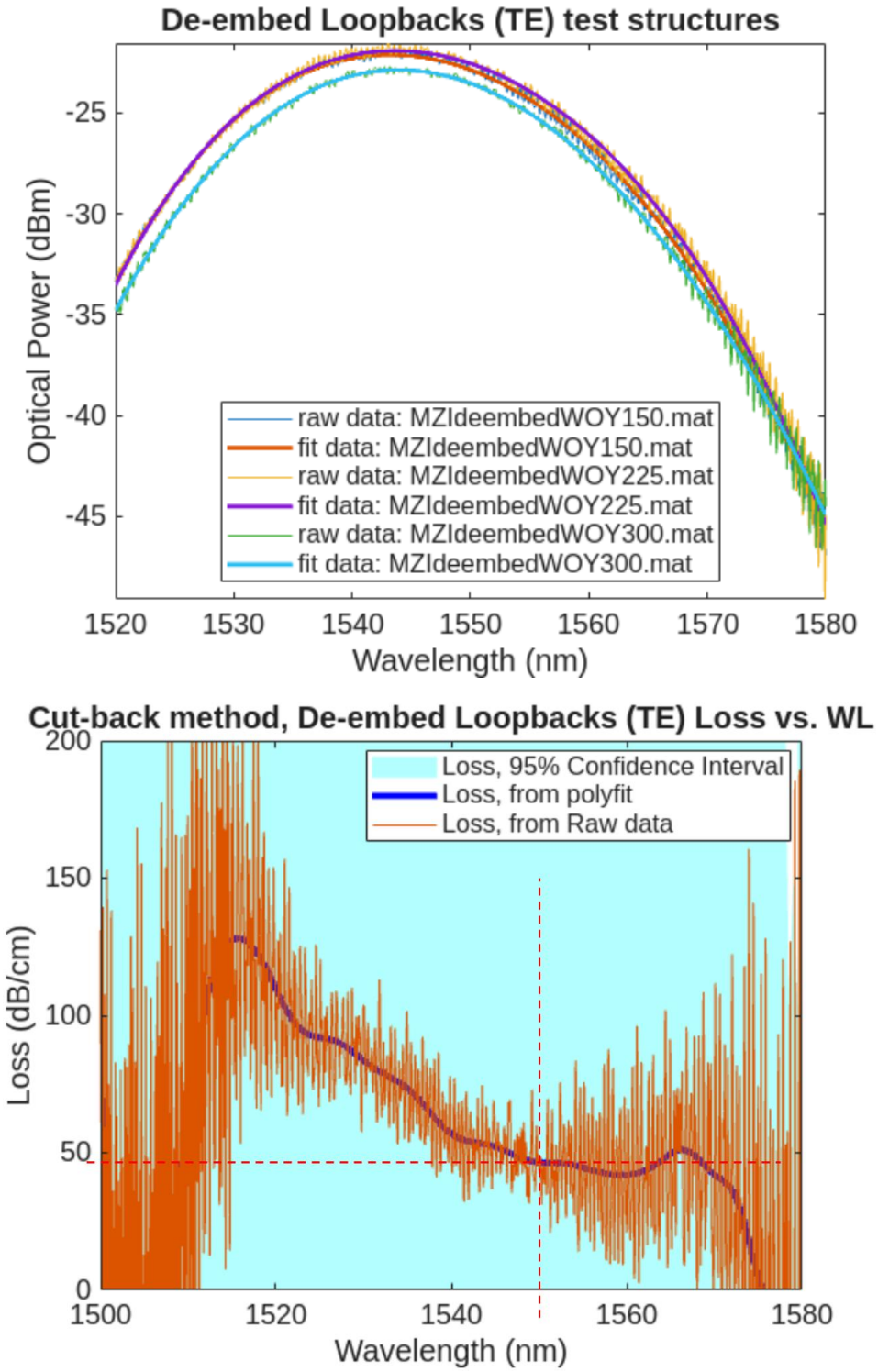


*Figure 11: Spectra of the de-embed loopbacks, and propagation loss from cutback analysis*

## 7. Conclusion

We report the theory, design, fabrication, and analysis of a range of unbalanced MZI's on a silicon photonic chip. The waveguides were modeled with Lumerical MODE software, and the MZI's modeled with Lumerical INTERCONNECT software. The layout for fabrication was performed using KLayout software, and the fabrication done using electron beam lithography at Applied Nanotools Inc in Edmonton, Canada. The devices were measured using a custom automated system at the University of British Columbia, and data analyzed using MATLAB software. There is good agreement (<1%) between simulated and experimental results, and they lie within the uncertainty from manufacturing variability.

## 8. Acknowledgment

We acknowledge the edX UBCx Phot1x Silicon Photonics Design, Fabrication and Data Analysis course, which is supported by the Natural Sciences and Engineering Research Council of Canada (NSERC) Silicon Electronic-Photonic Integrated Circuits (SiEPIC) Program. The devices were fabricated by Cameron Horvath at Applied Nanotools, Inc. Omid Esmaeeli performed the measurements at The University of British Columbia. We acknowledge Lumerical Solutions, Inc., Mathworks, Mentor Graphics, Python, and KLayout for the design software. Special thanks to professor Lukas Chrostowski for guidance and expertise.

## References


[1] R. J. Bojko, J. Li, L. He, T. Baehr-Jones, M. Hochberg, and Y. Aida, "Electron beam lithography writing strategies for low loss, high confinement silicon optical waveguides," J. Vacuum Sci. Technol. B 29, 06F309 (2011)

[2] Lukas Chrostowski, Michael Hochberg, chapter 12 in "Silicon Photonics Design: From Devices to Systems", Cambridge University Press, 2015

[3] http://siepic.ubc.ca/probestation, using Python code developed by Michael Caverley.

[4] Yun Wang, Xu Wang, Jonas Flueckiger, Han Yun, Wei Shi, Richard Bojko, Nicolas A. F. Jaeger, Lukas Chrostowski, "Focusing sub-wavelength grating couplers with low back reflections for rapid prototyping of silicon photonic circuits", Optics Express Vol. 22, Issue 17, pp. 20652-20662 (2014) doi: 10.1364/OE.22.020652

[5] www.plcconnections.com, PLC Connections, Columbus OH, USA.

[6] http://mapleleafphotonics.com, Maple Leaf Photonics, Seattle WA, USA.

[7] https://www.appliednt.com/nanosoi-fabrication-service/, Applied Nanotools, Edmonton, Canada